

Finite Element Analysis of MHD Unsteady Heat and Mass Transfer of Casson Nanofluid Flow over a Vertical Porous Plate Subjected to Thermal Radiation

M. G. Sobamowo

Department of Mechanical Engineering, University of Lagos, Akoka, Lagos State, Nigeria.
Email Address: gsobamowo@unilag.edu.ng

Article Info

Received: 28 June 2020

Revised: 12 August 2020

Accepted: 05 September 2020

Available online: 06 January 2021

Abstract

In this present study, finite element method is applied to analyze the magnetohydrodynamic transient heat and mass transfer of Casson nanofluid past an isothermal vertical flat plate embedded in a porous medium under the influence of thermal radiation is studied. The numerical solutions are used to carry out parametric studies. The parametric studies based on the numerical simulation reveal that the temperature as well as the concentration of the fluid increase as the Casson fluid and radiation parameters as well as Prandtl and Schmidt numbers increase. The increase in the Grashof number, radiation, buoyancy ratio and flow medium porosity parameters causes the velocity of the fluid to increase. However, the Casson fluid parameter, buoyancy ratio parameter, the Hartmann (magnetic field parameter), Schmidt and Prandtl numbers decrease as the velocity of the flow increases. The time to reach the steady state concentration, the transient velocity, Nusselt number and the local skin-friction decrease as the buoyancy ratio parameter and Schmidt number increase. Also, the steady-state temperature and velocity decrease as the buoyancy ratio parameter and Schmidt number increase. Also, the local skin friction, Nusselt and Sherwood numbers decrease as the Schmidt number increases. Though, the local Nusselt number increases as the buoyancy ratio parameter increases. It was established that near the leading edge of the plate, the local Nusselt number is not affected by both buoyancy ratio parameter and Schmidt number. The study provides better physical insight to the flow problem under the influence of thermal radiation and mass transfer as applied in various engineering processes.

Keywords and Phrases: Finite element method; Transient Free convection; Casson Nanofluid; Thermal radiation; Mass transfer.

MSC2010: 74F10

1 Introduction

There have been wide industrial and engineering applications of free convection flow over vertical surfaces. Such applications could be witnessed in mechanical forming processes, glass-fibre production processes, extrusion, food processing, melt spinning etc. Consequently, this has aroused lots

of research interests on the flow phenomena following the experimental investigations of Schmidt and Beckmann [1] and the pioneering theoretical work of Ostrach [2]. An extended work was done by Sparrow and Gregg [3] on the free convection under the influence of a uniform surface heat flux. In another work, the same authors [4] studied the flow phenomena over a non-isothermal vertical plate. Lefevre [5] examined the free convection of an inviscid flow under low Prandtl-numbers while Stewartson and Jones [6] as well as Eshghy [7] analyzed the flow over a heated vertical plate at high Prandtl number. Although, Roy [8] also studied the free convection flow process under a large Prandtl number, the effects of uniform surface heat flux on the flow phenomena was also investigated. Kuiken [9], [10] and Kuiken and Rotem [11] examined the free convection flow over the vertical plates at both low and high Prandtl numbers.

In recent times, different analytical and numerical methods have been used to examine the laminar free convection [12–18]. Also, various parametric studies on the nonlinear models and fluid flow problems have been presented in literature [19–28].

Different types of fluid such as tomato sauce, honey, printing inks, blood, concentrated fruit juices and Jelly have been classified as the non-Newtonian fluids called Casson fluids as invented by Casson [29]. These fluids exhibit shear thinning nature with an assumed infinite viscosity at zero rate of shear, a yield stress below which no flow occurs, and a zero viscosity at an infinite rate of shear [30]. Its important areas of applications have provoked some studies [30,31]. Also, the effects of thermal radiation, magnetic field and nanoparticles on the fluid flow processes have been extensively studied [33–41]. However, most of these studies which are based on time invariant, focused on the free convection currents caused by the temperature difference. It should be stated that the flow is also affected by the differences in concentration on material constitution such as seen in atmospheric flows, chemical processing, formation and dispersion of fog, distributive temperature and moisture over agricultural fields. Also, the transient behaviours of the fluids flow before a steady state is reached should be well investigated. Hence, the study of the transient heat and mass transfer of the fluid over the vertical plate is very much important. Moreover, to the best of the authors knowledge, a study on finite element analysis of transient behaviours of free convection boundary-layer flow, heat and mass transfer of Casson nanofluids over a vertical plate under the influences of thermal radiation, magnetic field, flow medium porosity and nanoparticles has not been presented in literature. Therefore, the transient magnetohydrodynamics free convection heat and mass transfer of Casson nanofluid past an isothermal vertical flat plate embedded in a porous media subjected to thermal radiation is studied using finite element method. Also, graphical presentation of the controlling parameters on the profiles of velocity, concentration and temperature are given and discussed.

2 Problem Formulation and Mathematical analysis

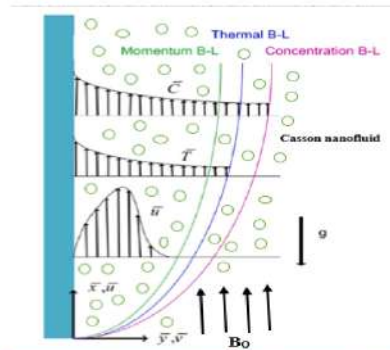


Fig. 1. Boundary layers for momentum, temperature and concentration profiles in the convection flow of a Casson fluid over a vertical plate.

In order to set up the flow, heat and mass transfer of the Casson nanofluid, the following assumptions are made

- i The flow is incompressible and laminar
- iii Pressure is uniform across the boundary layer and Boussinesq approximation is used
- iv The thermal diffusion and diffusion thermal effects which are called the Soret and Dufour effects, respectively are insignificant and they are therefore negligible.
- v The effect of viscous dissipation on the fluid flow process is negligible
- vi There is no chemical reaction taking place in the mass of the fluid.

Taken x -coordinate to be directed upward along the plate in the flow direction and y -coordinate is taken normal to the plate. Then under the stated assumptions, the governing equations of the flow, heat and mass transfer could be written as

$$\frac{\partial \bar{u}}{\partial x} + \frac{\partial \bar{v}}{\partial y} = 0 \quad (2.0.1)$$

$$\rho_{nf} \left(\frac{\partial \bar{u}}{\partial t} + \bar{u} \frac{\partial \bar{u}}{\partial x} + \bar{v} \frac{\partial \bar{u}}{\partial y} \right) = \left(1 + \frac{1}{\gamma} \right) \mu_{nf} \frac{\partial^2 \bar{u}}{\partial y^2} + g(\rho\beta)_{nf} (\bar{T} - \bar{T}_\infty) + g(\rho\beta^*)_{nf} (\bar{C} - \bar{C}_\infty) - \sigma_{nf} B_0^2 \bar{u} - \frac{\mu_{nf} \bar{u}}{K_p}$$

$$(\rho c_p)_{nf} \left(\frac{\partial \bar{T}}{\partial t} + \bar{u} \frac{\partial \bar{T}}{\partial x} + \bar{v} \frac{\partial \bar{T}}{\partial y} \right) = k_{nf} \frac{\partial^2 \bar{T}}{\partial y^2} - \frac{\partial q_r}{\partial y} \quad (2.0.2)$$

$$\left(\frac{\partial \bar{C}}{\partial t} + \bar{u} \frac{\partial \bar{C}}{\partial x} + \bar{v} \frac{\partial \bar{C}}{\partial y} \right) = D_{nf} \frac{\partial^2 \bar{C}}{\partial y^2} \quad (2.0.3)$$

In this work, we adopt a conditions that the plate and the fluid are initially at the same concentration and temperature level that is the same in the fluid everywhere. Then at time $t > 0$, the plate

temperature is suddenly raised to T_∞ , and the concentration level near the plate is also raised to C_∞ , which are thereafter maintained constant. Therefore, the initial condition is given as

$$\bar{t} \leq 0, \bar{u} = 0, \bar{v} = 0, T = T_\infty, C = C_\infty \text{ at } 0 \leq \bar{x} \leq L, \bar{y} \geq 0 \quad (2.0.4)$$

and the appropriate boundary conditions under no slip conditions are given as

$$\bar{t} > 0, \bar{u} = 0, \bar{v} = 0, T = T_\infty, C = C_\infty \text{ at } \bar{x} = 0, \bar{y} \geq 0 \quad (2.0.5)$$

$$\bar{t} > 0, \bar{u} = 0, \bar{v} = 0, T = T_\infty, C = C_\infty \text{ at } \bar{x} = L, \bar{y} \geq 0 \quad (2.0.6)$$

$$\bar{t} > 0, \bar{u} = 0, \bar{v} = 0, T = T_w, C = C_w \text{ at } \bar{x} \geq 0, \bar{y} = 0 \quad (2.0.7)$$

$$\bar{t} > 0, \bar{u} = 0, \bar{v} = V_\infty, T = T_\infty, C = C_\infty \text{ at } \bar{x} \geq 0, \bar{y} \rightarrow \infty \quad (2.0.8)$$

The thermal radiation term in Eq. (2.3) could be linearized using Rosseland's approximation as follows

$$\frac{\partial q_r}{\partial \bar{y}} = -\frac{4\sigma}{3K} \frac{\partial \bar{T}^4}{\partial \bar{y}} \cong -\frac{16\sigma T_s^3}{3K} \frac{\partial^2 \bar{T}}{\partial \bar{y}^2} \quad (2.0.9)$$

Substituting Eq. (2.10) into Eq. (2.3), we the governing equations of the flow, heat and mass transfer as

$$\frac{\partial \bar{u}}{\partial \bar{x}} + \frac{\partial \bar{v}}{\partial \bar{y}} = 0 \quad (2.0.10)$$

$$\begin{aligned} \rho_{rf} \left(\frac{\partial \bar{u}}{\partial \bar{t}} + \bar{u} \frac{\partial \bar{u}}{\partial \bar{x}} + \bar{v} \frac{\partial \bar{u}}{\partial \bar{y}} \right) &= \left(1 + \frac{1}{\gamma} \right) \mu_{rf} \frac{\partial^2 \bar{u}}{\partial \bar{y}^2} + g(\rho\beta)_{rf} (\bar{T} - \bar{T}_\infty) \\ &+ g(\rho\beta^*)_{rf} (\bar{C} - \bar{C}_\infty) - \sigma_{rf} B_0^2 \bar{u} - \frac{\mu_{rf} \bar{u}}{K_p} \end{aligned}$$

$$(\rho c_p)_{rf} \left(\frac{\partial \bar{T}}{\partial \bar{t}} + \bar{u} \frac{\partial \bar{T}}{\partial \bar{x}} + \bar{v} \frac{\partial \bar{T}}{\partial \bar{y}} \right) = \left(k_{rf} + \frac{16\sigma T_\infty^3}{3K} \right) \frac{\partial^2 \bar{T}}{\partial \bar{y}^2} \quad (2.0.11)$$

$$\left(\frac{\partial \bar{C}}{\partial \bar{t}} + \bar{u} \frac{\partial \bar{C}}{\partial \bar{x}} + \bar{v} \frac{\partial \bar{C}}{\partial \bar{y}} \right) = D_{rf} \frac{\partial^2 \bar{C}}{\partial \bar{y}^2} \quad (2.0.12)$$

where the various physical and thermal properties in Eqs. (2.13) and (2.14) are given as

$$\rho_{nf} = \rho_f(1 - \phi) + \rho_s\phi \quad (2.0.13)$$

$$(\rho c_p)_{nf} = (\rho c_p)_f(1 - \phi) + (\rho c_p)_s\phi \quad (2.0.14)$$

$$(\rho\beta)_{nf} = (\rho\beta)_f(1 - \phi) + (\rho\beta)_s\phi \quad (2.0.15)$$






$$\mu_{nf} = \frac{\mu_f}{(1 - \phi)^{2.5}} \quad (2.0.16)$$

$$\sigma_{nf} = \sigma_f \left[1 + \frac{m \left(\frac{\sigma_s}{\sigma_f} - 1 \right) \varphi}{\left(\frac{\sigma_s}{\sigma_f} + (m - 1) \right) - \left(\frac{\sigma_s}{\sigma_f} - (m - 2) \right) \varphi} \right] \quad (2.0.17)$$

$$k_{nf} = k_f \left[\frac{k_s + (m-1)k_f - (m-1)\phi(k_f - k_s)}{k_s + (m-1)k_f + \phi(k_f - k_s)} \right] \quad (2.0.18)$$

where m in the above Hamilton Crosser's model in Eq. (2.20) is the shape factor which numerical values for different shapes are given in Table 1.

Table 1: The values of different shapes of nanoparticles [41, 42]

S/N	Name	Shape	Shape factor (m)	Sphericity(ν)
1	Sphere		3.0	1.000
2	Brick		3.7	0.811
3	Cylinder		4.8	0.625
4	Platelet		5.7	0.526
5	Lamina		16.2	0.185

We now introduce the following non-dimensional quantities

$$x = \frac{\bar{x}}{L}, y = \frac{\bar{y}}{L} G_L^{1/2}, u = \frac{\rho_{rf} \bar{u} L}{\mu_{rf} G_L^{1/2}}, v = \frac{\rho_{rf} \bar{v} L}{\mu_{rf} G_L^{1/4}}, T = \frac{T - T_\infty}{T_w - T_\infty}, C = \frac{\bar{C} - C_\infty}{C_w - C_\infty}, \tau = \frac{t v}{L^2} G_L^{1/2}, Ha = \frac{\sigma_{rf} B_0^2 L^2}{\mu_{rf} G_L^{1/2}}, G_L = \frac{\rho_{rf}^2 g \beta L^3 (T_w - T_\infty)}{\mu_{rf}^2}, Pr = \frac{\mu_{rf} C_{p,rf}}{k_{rf}}, R = \frac{k_{[rf]} K}{4 \sigma T_w^3}, Sc = \frac{\mu_{rf}}{\rho_{rf} D_{rf}}, \lambda = \frac{\beta (C_w - C_\infty)}{\beta (T_w - T_\infty)}, \frac{1}{Da} = \frac{L^2}{G_L^{1/4} K_p}$$

We have the dimensionless forms of the governing equations as

$$\frac{\partial u}{\partial x} + \frac{\partial v}{\partial y} = 0 \quad (2.0.19)$$

$$\frac{\partial u}{\partial t} + u \frac{\partial u}{\partial x} + v \frac{\partial u}{\partial y} = \left(1 + \frac{1}{\gamma}\right) \frac{\partial^2 u}{\partial y^2} + T + \lambda C - Hau - \frac{1}{Da} u \quad (2.0.20)$$

$$\frac{\partial T}{\partial t} + u \frac{\partial T}{\partial x} + v \frac{\partial T}{\partial y} = \frac{1}{Pr} \left(\frac{3R+4}{3R} \right) \frac{\partial^2 T}{\partial y^2} \quad (2.0.21)$$

$$\frac{\partial C}{\partial t} + u \frac{\partial C}{\partial x} + v \frac{\partial C}{\partial y} = \frac{1}{Sc} \frac{\partial^2 C}{\partial y^2} \quad (2.0.22)$$

The appropriate initial and boundary conditions are given as

$$\tau \leq 0, u = 0, v = 0, T = 0, C = 0 \text{ at } 0 \leq x \leq 1, y \geq 0 \quad (2.0.23)$$

$$\tau > 0, u = 0, v = 0, T = 0, C = 0 \text{ at } x = 0, y \geq 0 \quad (2.0.24)$$

$$\tau > 0, u = 0, v = 0, T = 0, C = 0 \text{ at } x = 1, y \geq 0 \quad (2.0.25)$$

$$\tau > 0, u = 0, v = 0, T = 1, C = 1 \text{ at } x \geq 0, y = 0 \quad (2.0.26)$$

$$\tau > 0, u = 0, v = V_\infty, T \rightarrow 1, C \rightarrow 1 \text{ at } x \geq 0, y \rightarrow 0 \quad (2.0.27)$$

3 Finite Element Analysis of the Transient

Equations (21) - (24) are systems of coupled non-linear ordinary differential equations. It is very difficult to develop exact analytical solutions for these non-linear equations. Therefore, in order to solve the equations, recourse is made to a finite element method. The procedures of the numerical method are outlined as follows:

- i Finite element discretization
- ii Generation of the element equations
- iii Assembly of element equations
- iv Imposition of boundary conditions
- v Solution of assembled equation

In order to apply finite element method to the systems of the coupled nonlinear equations, the governing equations are multiplied by weight functions and the integrations over an element domain are set to zero, the following variational formulations are obtained:

$$\int \int_{\Omega_e} N_i \left[\frac{\partial u}{\partial t} + u \frac{\partial u}{\partial x} + v \frac{\partial u}{\partial y} - \left(1 + \frac{1}{\gamma} \right) \frac{\partial^2 u}{\partial y^2} - T - \lambda C + Hau + \frac{1}{Da} u \right] dx dy = 0 \quad (3.0.1)$$

$$\int \int_{\Omega_e} N_i \left[\frac{\partial T}{\partial t} + u \frac{\partial T}{\partial x} + v \frac{\partial T}{\partial y} - \frac{1}{Pr} \left(\frac{3R+4}{3R} \right) \frac{\partial^2 T}{\partial y^2} \right] dx dy = 0 \quad (3.0.2)$$

$$\int \int_{\Omega_e} N_i \left[\frac{\partial C}{\partial t} + u \frac{\partial C}{\partial x} + v \frac{\partial C}{\partial y} - \frac{1}{Sc} \frac{\partial^2 C}{\partial y^2} \right] dx dy = 0 \quad (3.0.3)$$

The Galerkin finite element formulation may be obtained from Eq. (3.1)-(3.3) by substituting the finite element approximations of the form:

$$u = \sum_{j=1}^3 N_j u_j, T = \sum_{j=1}^3 N_j T_j, C = \sum_{j=1}^3 N_j C_j \quad (3.0.4)$$

where N_j are the linear interpolation functions for a triangular element, Ω_e .

It should be stated that the requirement on continuity of field variables is much stronger in its present strong forms in Eqs. (3.1) – (3.3). In order to overcome the difficulties, weak formulations are preferred. Indisputably, the weak formulations help to reduce the order of continuity needed for elements selected i.e. it will reduce the continuity requirements on the approximation (or basis functions) functions thereby allowing the use of easy-to-construct and implement polynomials. Moreover, weak formulation automatically enforces natural boundary conditions. Therefore, the desired weak forms of the variational formulations are developed by replacing the unknowns in the weighted residual approach in Eqs. (3.1) – (3.3) by approximate trial solutions which are given by polynomial relationships in Eq. (3.4) and carry out the integrations by parts over the element domain. Incorporating the boundary conditions directly into the weak forms after the integrations by parts over the element domain. The finite element model of the equations in matrix form is given as

$$\begin{bmatrix} [p^{11}] & [p^{12}] & [p^{13}] \\ [p^{21}] & [p^{22}] & [p^{23}] \\ [p^{31}] & [p^{32}] & [p^{33}] \end{bmatrix} \begin{bmatrix} \{\dot{u}\} \\ \{\dot{T}\} \\ \{\dot{C}\} \end{bmatrix} + \begin{bmatrix} [K^{11}] & [K^{12}] & [K^{13}] \\ [K^{21}] & [K^{22}] & [K^{23}] \\ [K^{31}] & [K^{32}] & [K^{33}] \end{bmatrix} \begin{bmatrix} \{u\} \\ \{T\} \\ \{C\} \end{bmatrix} = \begin{bmatrix} \{S^{(1)}\} \\ \{S^{(2)}\} \\ \{S^{(3)}\} \end{bmatrix} \quad (3.0.5)$$

where \dot{u} , \dot{T} and \dot{C} are the time derivatives of u , T and C , respectively. Also, $[p^{mn}]$, $[K^{mn}]$ and $[S^m]$ are defined as follows:

$$p_{ij}^{11} = \int \int_{\Omega_e} N_i N_j dx dy, \quad p_{ij}^{12} = 0, \quad p_{ij}^{13} = 0$$

$$K_{ij}^{11} = \int \int_{\Omega_e} N_i \bar{u} \frac{\partial N_j}{\partial x} dx dy + \int \int_{\Omega_e} N_i \bar{v} \frac{\partial N_j}{\partial y} dx dy + \left(Ha + \frac{1}{Da} \right) \int \int_{\Omega_e} N_i N_j dx dy + \left(1 + \frac{1}{\gamma} \right) \int \int_{\Omega_e} \frac{\partial N_i}{\partial y} \frac{\partial N_j}{\partial y} dx dy$$

$$K_{ij}^{12} = - \int \int_{\Omega_e} N_i N_j dx dy, \quad K_{ij}^{13} = -\lambda \int \int_{\Omega_e} N_i N_j dx dy, \quad S^{(2)}$$

$$p_{ij}^{21} = 0, \quad p_{ij}^{22} = \int \int_{\Omega_e} N_i N_j dx dy, \quad p_{ij}^{23} = 0$$

$$K_{ij}^{22} = \int \int_{\Omega_e} N_i \bar{u} \frac{\partial N_j}{\partial x} dx dy + \int \int_{\Omega_e} N_i \bar{v} \frac{\partial N_j}{\partial y} dx dy + \frac{1}{pr} \left(\frac{3R+4}{3R} \right) \int \int_{\Omega_e} \frac{\partial N_i}{\partial y} \frac{\partial N_j}{\partial y} dx dy$$

$$K_{ij}^{21} = 0, \quad K_{ij}^{23} = 0, \quad S^{(3)} = 0$$

$$p_{ij}^{31} = 0, \quad p_{ij}^{32} = 0, \quad p_{ij}^{33} = \int \int_{\Omega_e} N_i N_j dx dy$$

$$K_{ij}^{33} = \int \int_{\Omega_e} N_i \bar{u} \frac{\partial N_j}{\partial x} dx dy + \int \int_{\Omega_e} N_i \bar{v} \frac{\partial N_j}{\partial y} dx dy + \frac{1}{Sc} \int \int_{\Omega_e} \frac{\partial N_i}{\partial y} \frac{\partial N_j}{\partial y} dx dy$$

$$K_{ij}^{31} = 0, \quad K_{ij}^{32} = 0, \quad S^{(3)} = 0$$

where

$$\bar{u} = \sum_{j=1}^3 N_j \bar{u}_j, \quad \bar{v} = \sum_{j=1}^3 N_j \bar{v}_j$$

It should be stated that \bar{u} and \bar{v} are the assumed known incorporated functions that are used to linearize the system of equations.

With the aid of Crank-Nicolson scheme as in the author's previous study [46], the time derivatives are approximated. Then the computational domain is uniformly divided into 448 triangular elements of three nodes each. This makes the total number of nodes in the whole domain to be 285. Since, at each node, three functions are evaluated, then, the order of each element matrix is 9×9 . After assembly of the elemental equations, a system of 855 nonlinear coupled equations is initially obtained. The system of nonlinear coupled equations are linearized using and as stated above. After imposition of the boundary conditions into the system of linearized coupled equations, a system of 660 linear coupled equations (of order 660×660) are obtained. The linearized system of equations is solved by using Gauss Seidel iteration method. The convergence of solutions is assumed when the relative error for each variable between consecutive iterations is recorded below the convergence criterion such that $\sum |\phi_i^s - \phi_i^{s-1}| \leq 10^{-6}$, where ϕ is the general dependent variable u , T and C and s is the number of iteration.

4 Results and discussion

The results of the numerical simulations are presented. Grid independence and sensitivity analyses are carried out. The results with the discussion are illustrated through the Figs. 2-19 to substantiate the applicability of the present analysis.

4.1 Grid independency test and code verification

A mesh sensitivity analysis was carried out to ensure grid independence. In order to choose the grid size, grid independency test is performed for the grid mesh of sizes of 21×21 , 31×31 , 41×41 , 51×51 , 61×61 , 71×71 , 81×81 , 91×91 , 101×101 , 111×111 and 121×121 . It is observed that for large values of number of grids greater than 81×81 , there is no appreciable change in the results. It is observed that in the same domain the accuracy is not affected even if the numbers of elements are increased by decreasing the size of the elements. The grid independency test shows that a grid mesh of size 91×91 is adequate to describe the flow processes. Also, the results obtained for lesser number of elements are of sufficient accuracy. Hence the grid a grid mesh of size 91×91 can be used to get the results that accurately describe the flow and heat transfer processes.

The available results in literature verify the solution procedure, in the form of an in-house computational fluid dynamics code. Therefore, this method has been proven to be adequate and give accurate results for boundary layer problems as presented in this work.

4.2 Effects of Casson parameter on the fluid velocity, temperature and concentration distributions

The effects of Casson parameter on the flow velocity, temperature and concentrations profiles of the nanofluid are shown in Fig. 3a, 3b and 3c, respectively. The figures depict that the flow velocity of the nanofluid near the plate decreases as the Casson parameter increases as illustrated in Fig. 3a. The trend in the figure could explained that, physically, increasing values of Casson parameter develop the viscous forces which in consequent retards the flow of the and thereby reduced the flow velocity. It could be established from the results that the temperature as well as the concentration of the fluid increase as the Casson fluid parameter increase as shown in Fig. 3b and 3c.

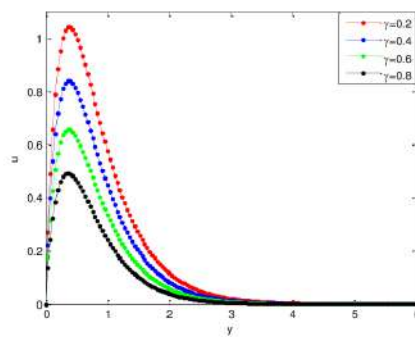


Fig. 3a. Effects of Casson parameter on the velocity profile of the Casson nanofluid

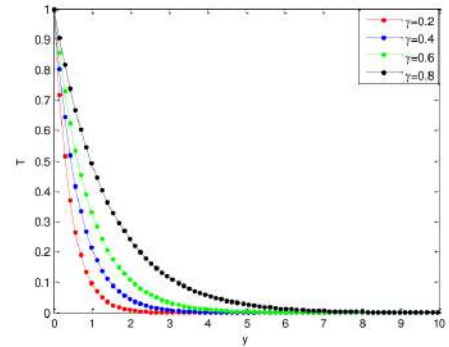


Fig. 3b. Effects of Casson parameter on temperature profile of the Casson nanofluid

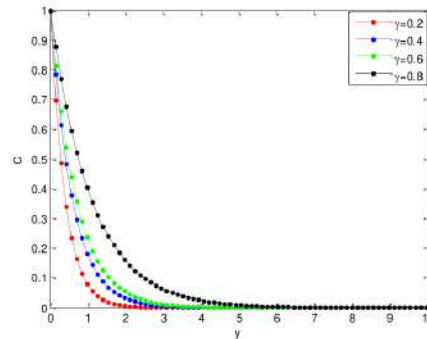


Fig. 3c. Effects of Casson parameter on concentration profile Of the Casson nanofluid

4.3 Effects of radiation parameter on the fluid velocity, temperature and concentration distributions

Fig. 4a, 4b and 4c show that the viscous, thermal and concentration boundary layers increase with the increase of radiation parameter, R . It is shown that increase in radiation parameter causes the velocity of the fluid to increase. This is because as the radiation parameter is increased, the absorption of radiated heat from the heated plate releases more heat energy released to the fluid and the resulting temperature increases the buoyancy forces in the boundary layer which also increases the fluid motion and the momentum boundary layer thickness accelerates. This is expected, because the considered radiation effect within the boundary layer increases the motion of the fluid which increases the surface frictions.

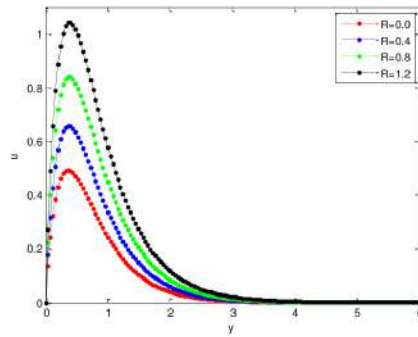


Fig. 4a. Effects of radiation parameter on the velocity profile of the Casson nanofluid

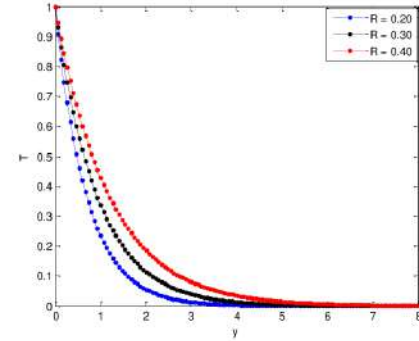


Fig. 4b. Effects of radiation parameter on temperature profile of the Casson nanofluid

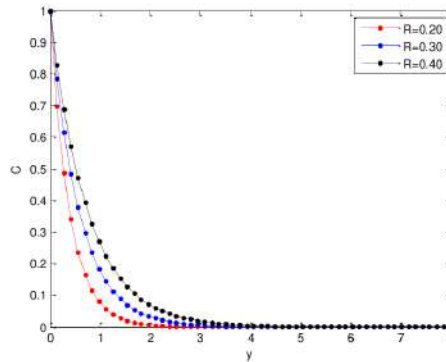


Fig. 4c. Effects of radiation parameter on concentration profile of the Casson nanofluid

4.4 Effects of nanoparticle shape on the fluid velocity, temperature and concentration distributions

The use of nanoparticles in the fluids exhibited better properties relating to the heat transfer of fluid than heat transfer enhancement through the use of suspended millimeter- or micrometer-sized particles which potentially cause some severe problems, such as abrasion, clogging, high pressure drop, and sedimentation of particles. The very low concentrations applications and nanometer sizes properties of nanoparticles in basefluid prevent the sedimentation in the flow that may clog the channel. It should be added that the theoretical prediction of enhanced thermal conductivity of the basefluid and prevention of clogging, abrasion, high pressure drop and sedimentation through the addition of nanoparticles in basefluid have been supported with experimental evidences in literature.

Fig. 5a, 5b and 5c show the influence of the shape of nanoparticle on the flow velocity, temperature

and concentrations profiles of the nanofluid. It is observed that lamina shaped nanoparticle carries maximum velocity whereas spherical shaped nanoparticle has better enhancement on heat transfer than other nanoparticle shapes. In fact, it is in accordance with the physical expectation since it is well known that the lamina nanoparticle has greater shape factor than other nanoparticles of different shapes, therefore, the lamina nanoparticle comparatively gains maximum temperature than others. The velocity decrease is maximum in spherical nanoparticles when compared with other shapes. The enhancement observed at lower volume fractions for non-spherical particles is attributed to the percolation chain formation, which perturbs the boundary layer and thereby increases the local Nusselt number values. The results show that the maximum decrease in velocity and maximum increase in temperature are caused by lamina, platelets, cylinder and sphere, respectively. It is also observed that irreversibility process can be reduced by using nanoparticles, especially the spherical particles. This can potentially result in higher enhancement in the thermal conductivity of a nanofluid containing elongated particles compared to the one containing spherical nanoparticle, as exhibited by the experimental data in the literature. It is therefore required that proper choice of nanoparticles should be made as this will be helpful in controlling fluid flow, heat and mass transfer processes

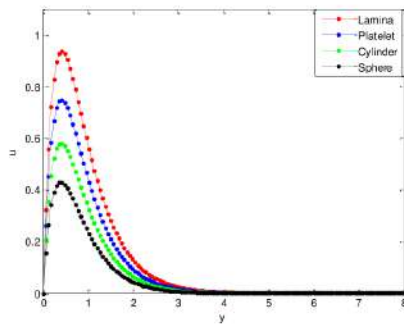


Fig. 5a. Effect of nanoparticle shape on velocity distribution of the nanofluid

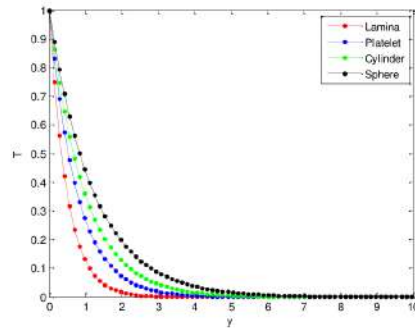


Fig. 5b. Effects of nanoparticle shape on temperature distribution of nanofluid

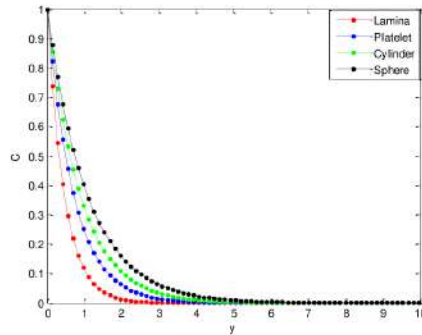


Fig. 5c. Effects of nanoparticle shape on concentration distribution

4.5 Effect of Prandtl number on the fluid velocity, temperature and concentration distributions

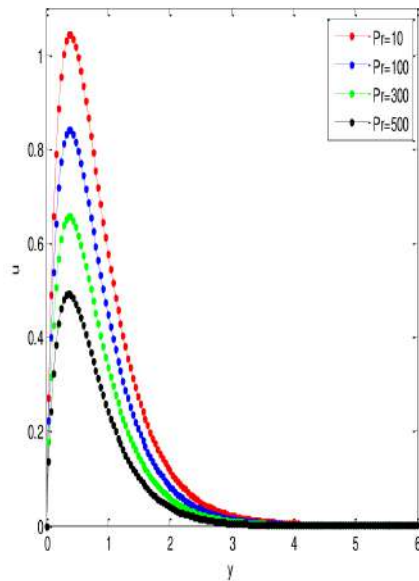


Fig. 6a. Effects of Prandtl number on the velocity profile

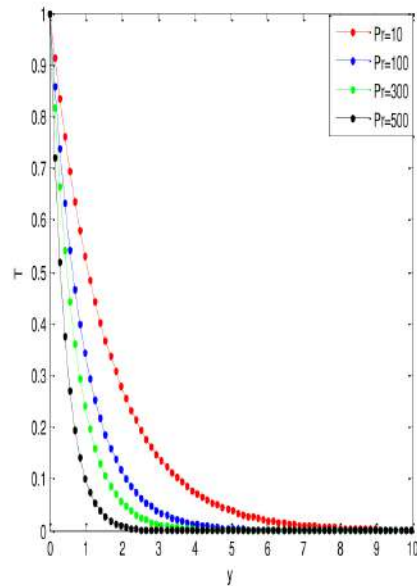


Fig. 6b. Effects of Prandtl number on temperature profile

The figures also show the effects of Prandtl number (Pr) on the velocity and temperature profiles are shown in Fig. 6a, 6b and 6c, respectively. It is indicated that the velocity of the Casson nanofluid decreases as the Pr increases but the temperature of the nanofluid increases as the Pr increases. This is because the nanofluid with higher Prandtl number has a relatively low thermal conductivity, which reduces conduction, and thereby reduces the thermal boundary-layer thickness, and as a consequence, increases the heat transfer rate at the surface. For the case of the fluid velocity that decreases with the increase of Pr , the reason is that fluid of the higher Prandtl number means more viscous fluid, which increases the boundary-layer thickness and thus, reduces the shear stress and consequently, retards the flow of the nanofluid. Also, it can be seen that the velocity distribution for small value of Prandtl number consist of two distinct regions. A thin region near the wall of the plate where there are large velocity gradients due to viscous effects and a region where the velocity gradients are small compared with those near the wall. In the later region, the viscous effects are negligible and the flow of fluid in the region can be considered to be inviscid. Also, such region tends to create uniform accelerated flow at the surface of the plate.

4.6 4.6 Effect of Schmidt and Grashof numbers on fluid velocity and temperature distributions

Fig. 7a and 7b show the effects of Schmidt number (Sc) on the velocity and concentration profiles of the Casson nanofluid, respectively. Fig. 8 shows that the as Grashof number increases, the velocity of the fluid increases. However, as in the case of the effect of Prandtl number on the velocity and temperature distribution, it is depicted in the figures that the velocity of the nanofluid decreases as the Sc increases but the temperature of the nanofluid increases as the Sc increases. This is because the nanofluid with higher Schmidt number has a relatively low diffusion coefficient, which reduces mass diffusion thereby reduces the concentration boundary-layer thickness, and as a consequence, increases the mass transfer rate at the surface. In Fig. 7a, where the fluid velocity decreases with the increase of Sc , this is because the fluid of the higher Schmidt number means more viscous fluid, which increases the boundary-layer thickness and thus, reduces the shear stress and consequently, retards the flow of the nanofluid. It is also observed that the species concentration decreases with increasing Schmidt number as shown in Fig. 7b. It was also found that the temperature increases with increasing Schmidt number. A further investigation revealed that an increase in the Schmidt number leads to a decrease in Grashof number Gr .

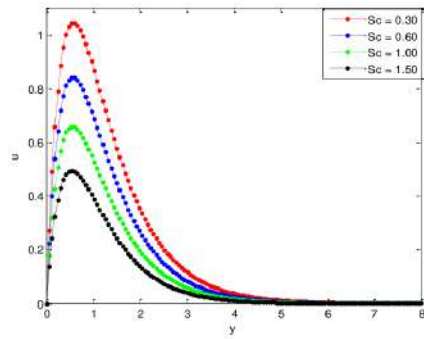


Fig. 7a. Effects of Schmidt number on the velocity distribution

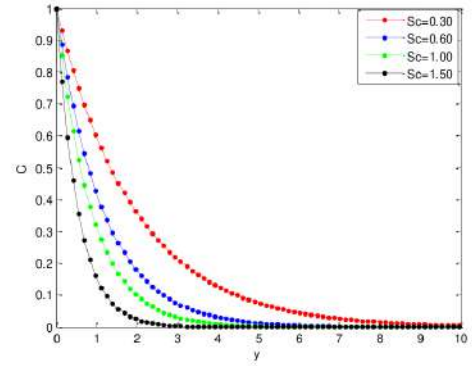


Fig. 7b. Effects of Schmidt number on the concentration distribution

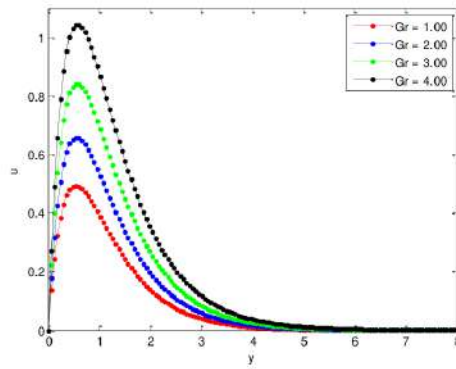


Fig. 8. Effects of Grashof number on the velocity distribution

4.7 Effects of Magnetic field and Flow Medium Porosity on Casson nanofluid velocity distributions

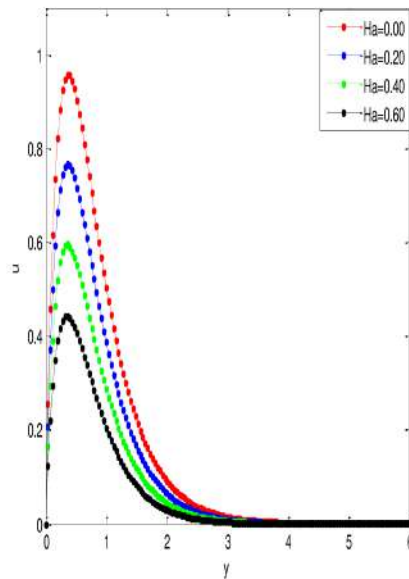


Fig. 9. Effects of Hartmann number on the velocity distribution

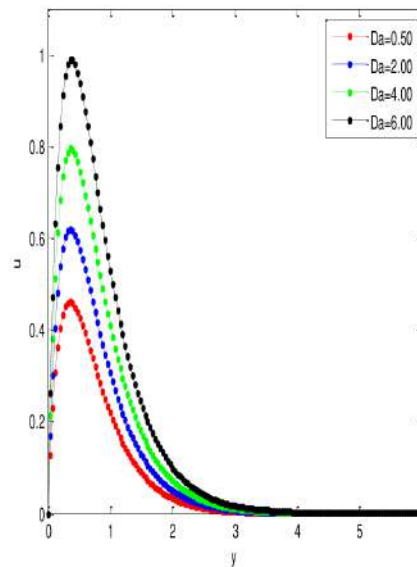


Fig. 10 Effects of Darcy number on the concentration distribution

Figs. 9 shows the effect of magnetic field on the flow velocity of the fluid. It is revealed that there is a diminution in the velocity field occurs for increasing value of the magnetic field number, Hartmann number (Ha). This confirms the general physical behavior of the magnetic field that say that the fluid velocity depreciates for improved values of Ha . The magnetic field produces Lorentz force which is drag-like force that produces more resistance to the flow and reduces the fluid velocity. So large Ha values implies that the Lorentz force increases and the resistance to the flow increases, and consequently, the velocity of the fluid decreases. Practically, the Lorentz force has a resistive nature which opposes motion of the fluid and as a result heat is produced which increases thermal boundary layer thickness and fluid temperature. The magnetic field tends to make the boundary layer thinner, thereby increasing the wall friction. Consequently, the boundary layer thickness is a decreasing function of Ha . i.e. presence of magnetic field slows fluid motion at boundary layer and hence retards the velocity field.

A porous medium studies is very important in a number of engineering applications such as geophysics, die filling, metal processing, agricultural and industrial water distribution, oil recovery techniques, and injection molding. Therefore, Figs. 10 shows the effect of flow medium porosity on the fluid velocity. As it is illustrated, the fluid velocity increases as the flow medium porosity, Darcy number increases. This is because, as the Darcy number increases, there is less resistance to fluid flow through the flow medium.

4.8 Effect of Buoyancy ratio parameter on the fluid velocity, temperature and concentration distributions

Fig 11a, 11b and 11c show the impacts of buoyancy ratio parameter ($N = \lambda$) on the velocity, temperature and concentration profiles. Fig. 11a depicts that the as buoyancy ratio parameter increases, the velocity of the fluid increases. However, an increase in buoyancy ratio parameter leads to a decrease in the fluid temperature and concentration as shown in Figs. 11b and 11c

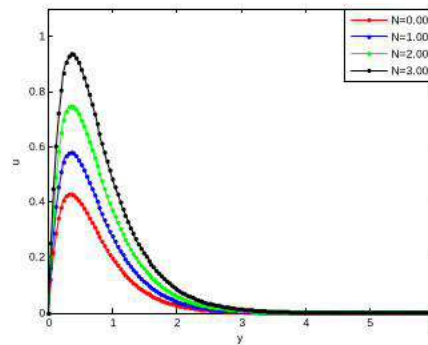


Fig. 11a. Effects of buoyancy ratio on the velocity distribution

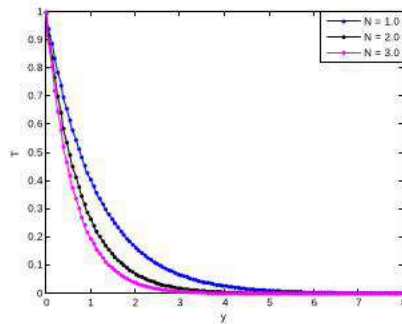


Fig. 11b. Effects of buoyancy ratio on the temperature distribution

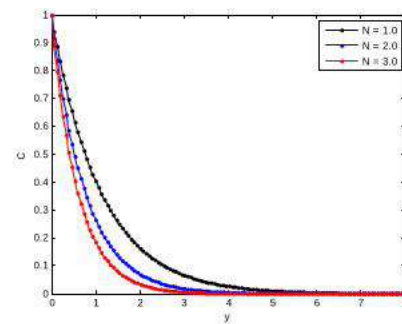


Fig. 11c. Effects of buoyancy ratio on the concentration distribution

4.9 Effect of flow time on the fluid velocity, temperature and concentration distributions

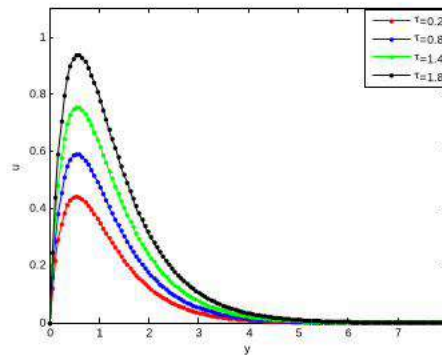


Fig. 12a. Effects of flow time on the velocity distribution

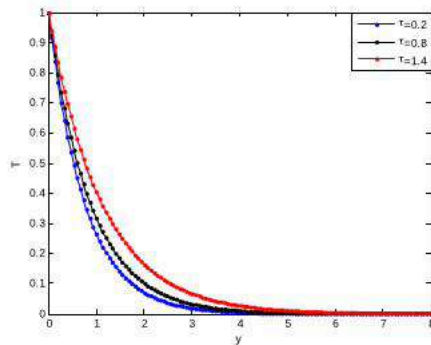


Fig. 12b. Effects of flow on the temperature distribution

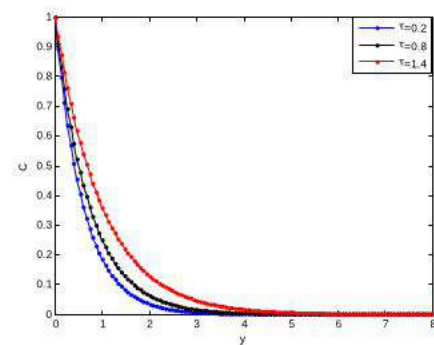


Fig. 12c. Effects of flow time on the concentration distribution

In order to show the effects of flow time on the velocity, temperature and concentration distributions, Figs. 11a-c are presented. Apart from the fact that the velocity, temperature and concentration distributions increase as the flow time increases, the results also show the effects of the controlling parameters on the time to reach steady state velocity, temperature and concentration. In our further investigations, the required time to reach the steady state concentration, the transient velocity, Nusselt number and the local skin-friction decrease as the buoyancy ratio parameter and Schmidt number increase. Also, the steady-state temperature and velocity decrease as the buoyancy ratio parameter and Schmidt number increase.

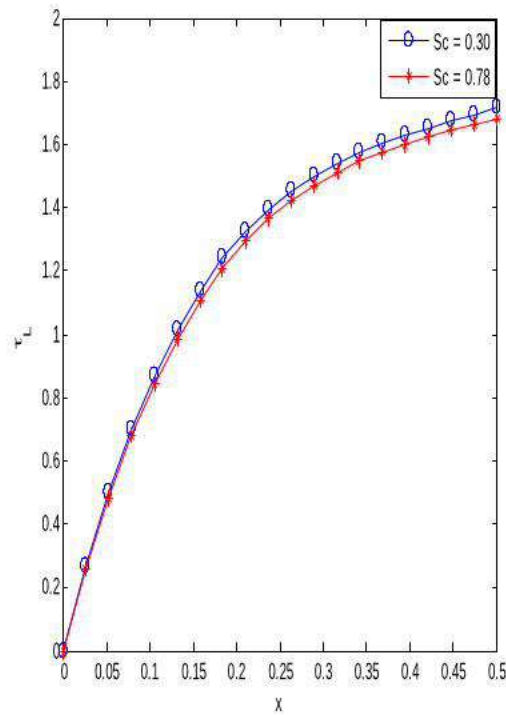


Fig. 13. Effects of Schmidt number on local skin friction

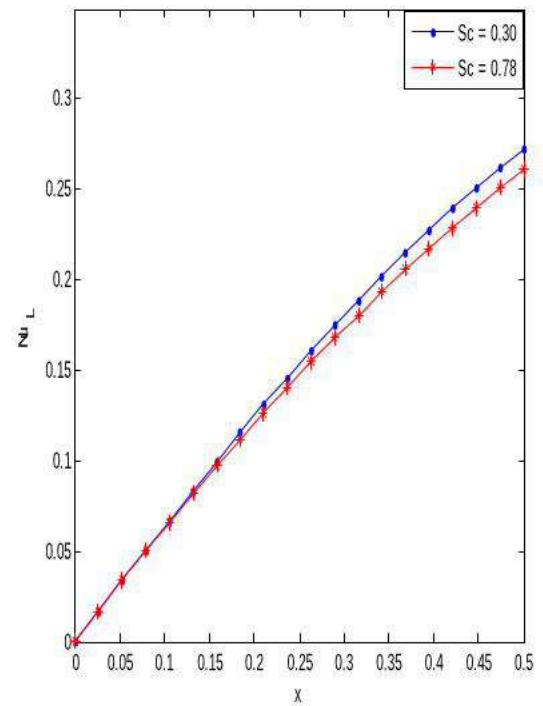


Fig. 14. Effects of Schmidt number on Nusselt number

The effects of Schmidt number on local skin friction, Nusselt and Sherwood numbers are shown in Fig. 13, 14 and 15, respectively. The figures reveal that the local skin friction, Nusselt and Sherwood numbers decrease as the Schmidt number increases. An opposite trend was recorded when the impact of the buoyancy ratio parameter on Nusselt number was investigated. In the investigation, it was found that as the local Nusselt number increases as the buoyancy ratio parameter increases. It was shown that at small values of x (near the leading edge of the plate), the local Nusselt number is not affected by both buoyancy ratio parameter and Schmidt number due to the pure diffusion and conduction at the location.

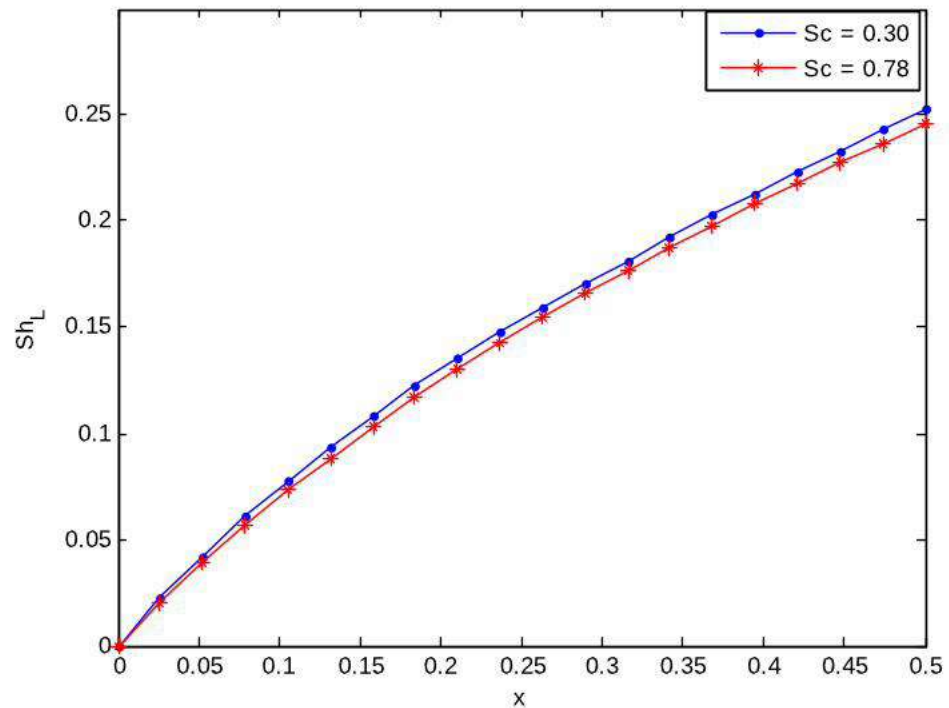


Fig. 15. Effects of Schmidt number on Sherwood number

5 Conclusion

In this present study, the transient free convection heat and mass transfer of Casson nanofluid past an isothermal vertical flat plate embedded in a porous medium under the influences of thermal radiation and magnetic field have been investigated. The governing systems of nonlinear partial differential equations of the flow, heat and mass transfer processes are solved using implicit finite difference scheme of Crank-Nicolson type. The numerical solutions are used to carry out parametric studies and the follow results were established:

- i The temperature and the concentration of the fluid increase as the Casson fluid and radiation parameters as well as Prandtl and Schmidt numbers increase.
- ii The increase in the Grashof number, radiation, buoyancy ratio and flow medium porosity parameters causes the velocity of the fluid to increase. However, the Casson fluid parameter,

buoyancy ratio parameter, the Hartmann (magnetic field parameter), Schmidt and Prandtl numbers decrease as the velocity of the flow increases.

- iii The time to reach the steady state concentration, the transient velocity, Nusselt number and the local skin-friction decrease as the buoyancy ratio parameter and Schmidt number increase.
- iv The steady-state temperature and velocity decrease as the buoyancy ratio parameter and Schmidt number increase.
- v The local skin friction, Nusselt and Sherwood numbers decrease as the Schmidt number increases. However, the local Nusselt number increases as the buoyancy ratio parameter increases.
- vi The maximum decrease in velocity and maximum increase in temperature in the nanofluid flow are caused by lamina, platelets, cylinder and sphere, respectively.

Following the results in this work, it is believed that the present study will greatly assist in various areas of industrial and engineering applications of the flow problems.

Nomenclature, Symbols & Subscrip

B_0	electromagnetic induction	R	Radiation number
c_p	specific heat capacity	S_c	Schmidt number
C	species concentration	t	time
D	species diffusion coefficient	\bar{T}	temperature of the fluid
g	acceleration due to gravity	\bar{u}	velocity component in x-direction
G_r	Grashof number	\bar{v}	velocity component in y-direction
H_a	Hartmann number/magnetic field parameter	U_w	fluid inflow velocity at the wall
k	thermal conductivity	\bar{x}	coordinate axis parallel to the plate
K	the absorption coefficient	\bar{y}	coordinate axis perpendicular to the plate
m	shape factor	β	volumetric extension coefficients
N	buoyancy ratio parameter	ρ_{nf}	density of the nanofluid
P_r	Prandtl number	σ_{nf}	permeability of the magnetic field
\underline{p}_r	Prandtl number	σ	Stefan-Boltzmann constant
\bar{P}	pressure	f	fluid
P	pressure	s	solid
ρ_f	density of the base fluid	nf	nanofluid
μ_{nf}	dynamic viscosity of the nanofluid	w	wall
ρ_s	density of the solid/nanoparticles		
ϕ	fraction of nanoparticles in the nanofluid		
γ	Casson parameter		
τ	shear stress		
τ_0	Casson yield stress		
μ	dynamic viscosity		

Acknowledgements

The author is grateful to the reviewers for their valuable suggestions and contributions on improving the paper.

Competing financial interests

The author declares no competing financial interests”.

References

- [1] Schmidt,E. & Beckmann,W. Das temperatur-und geschwindigkeitsfeldvoneinerwärmeabgebendenskenrecherplattebeinatürellicher convention. *Tech. Mech. U. Thermodynamik*, Bd. 1, 341–349, (1930).
- [2] Ostrach,S. An analysis of laminar free-convection flow and heat transfer about a flat plate parallel to the direction of the generating body force. *NACA Report* **1111**, (1953).
- [3] Sparrow,E.M. & Gregg,J.L. Laminar free convection from a vertical plate with uniform surface heat flux. *Trans. A.S.M.E.* **78**, 435–440, (1956).
- [4] Sparrow,E.M. & Gregg,J.L. Similar solutions for free convection from a nonisothermal vertical plate. *Trans. A.S.M.E.* **80**, 379–386, (1958).
- [5] Lefevre,E.J. Laminar free convection from a vertical plane surface. *9th Intern. Congress on Applied Mechanics, Brussels, paper I* **168**, (1956).
- [6] Stewartson,K. & Jones,L.T. The heated vertical plate at high Prandtl number. *J. Aeronautical Sciences* **24**, 379–380, (1957).
- [7] Eshghy,S. Free-convection layers at large Prandtl number. *J. Applied Math. and Physics (ZAMP)* **22**, 275–292, (1971).
- [8] Roy,S. High Prandtl number free convection for uniform surface heat flux. *Trans A.S.M.E.J. Heat Transfer* **95**, 124–126, (1973).
- [9] Kuiken,H.K. An asymptotic solution for large Prandtl number free convection. *J. Engng. Math.* **2**, 355–371, (1968).
- [10] Kuiken,H.K. Free convection at low Prandtl numbers. *J. Fluid Mech.* **37**, 785–798, (1969).
- [11] Kuiken,H.K.& Rotem,Z. Asymptotic solution for the plume at very large and small Prandtl numbers. *J. Fluid Mech.* **45**, 585–600, (1971).
- [12] Na,T.Y.& Habib,I.S. Solution of the natural convection problem by parameter differentiation. *Int. J. Heat Mass Transfer* **17**, 457–459, (1974).
- [13] Merkin,J.H. A note on the similarity solutions for free convection on a vertical plate. *J. Engng. Math.* **19**, 189–201, (1985).
- [14] Merkin,J.H.& Pop,I. Conjugate free convection on a vertical surface. *Int. J. Heat Mass Transfer* **39**, 1527–1534, (1996).
- [15] Ali,F.M., Nazar,R.& Arifin,N.M. Numerical investigation of free convective boundary layer in a viscous fluid. *The American Journal of Scientific Research* **5**, 13–19, (2009).
- [16] Motsa,S.S.,Shateyi,S.& Makukula,Z. Homotopy analysis of free convection boundary layer flow with heat and mass transfer. *Chemical Engineering Communications* **198**, 783–795, (2011).
- [17] Motsa,S.S., Makukula,Z.G.& Shateyi,S. Spectral Local Linearisation Approach for Natural Convection Boundary Layer Flow. *Hindawi Publishing Corporation Mathematical Problems in Engineering* **2013**, 1–7, (2013).
- [18] Ghotbi,A.R.,Bararnia,H., Domairry,G.& Barari,A. Investigation of a powerful analytical method into natural convection boundary layer flow. *Communications in Nonlinear Science and Numerical Simulation* **14**, 2222–2228, (2009).

- [19] Mosayebidorcheh,S.& Mosayebidorcheh,T. Series solution of convective radiative conduction equation of the nonlinear fin with temperature dependent thermal conductivity. *International Journal of Heat and Mass Transfer* **55**, 6589–6594, (2012).
- [20] Sheikholeslami,M. CVFEM for magnetic nanofluid convective heat transfer in a porous curved enclosure. *The European Physical Journal Plus* **2016**, 131–413, (2016).
- [21] Sheikholeslami,M.& Ganji,D.D. Hydrothermal Analysis in Engineering Using Control Volume Finite Element Method. *First edition, Elsevier* .
- [22] Sheikholeslami,M. Application of Control Volume Based Finite Element Method (CVFEM) for Nanofluid Flow and Heat Transfer. *First edition, Elsevier* .
- [23] Sheikholeslami,M. Numerical study of MHD Natural convection liquid metal flow and heat transfer in a wavy enclosure using CVFEM. *Heat Transfer Research* **48**, 121–138, (2017).
- [24] Mosayebidorcheh,S., Rahimi-Gorji,M., Ganji,D.D., T. Moayebidorcheh, O. Pourmehran& M. Biglarian Transient thermal behavior of radial fins of rectangular, triangular and hyperbolic profiles with temperature-dependent properties using DTM-FDM. *Journal of Central South University* **24**, 675–682, ().
- [25] Mosayebidorcheh,S. , Makinde,O.D., Ganji,D.D.& Chermahini,M.A. DTM-FDM hybrid approach to unsteady MHD Couette flow and heat transfer of dusty fluid with variable properties. *Thermal Science and Engineering Progress* **2**, 57–63, ().
- [26] Mosayebidorcheh,S., Farzinpoor,M.& Ganji,D.D. Transient thermal analysis of longitudinal fins with internal heat generation considering temperature-dependent properties and different fin profiles. *Energy Conversion and Management* **86**, 365–370, (2014)
- [27] Mosayebidorcheh,S., Rashidi,M.M.& Moayebidorcheh,T. Analytical solution of the steady state condensation film on the inclined rotating disk by a new hybrid method. *Scientific Research and Essays* **9**, 557–565, ()
- [28] Mosayebidorcheh,S., Vatani,M.M., Ganji,D.D.& Moayebidorcheh,T. Investigation of the viscoelastic flow and species diffusion in a porous channel with high permeability. *Alexandria Engineering Journal* **53**, 779–785, ()
- [29] N. Casson Rheology of Dispersed System. *Pergamon Press, Oxford, UK* **84**, (1959).
- [30] Dash,R.K., Mehta,K.N.& Jayaraman,G. Casson fluid flow in a pipe filled with a homogeneous porous medium. *International Journal of Engineering Science* **34**, 1145–1156, (1996).
- [31] Eldabe,N.T.M.& Salwa,M.G.E. Heat transfer of mhd non-Newtonian Casson fluid flow between two rotating cylinder. *Journal of the Physical Society of Japan* **64**, 41–64, (1995).
- [32] Nadeem,S., Haq,R.L., Akbar,N.S.& Khan,Z.H. MHD three-dimensional Casson fluid flow past a porous linearly stretching sheet. *Alexandria. Engineering Journal* **52**, 577–582, (2013).
- [33] Raptis,A.& Perdikis,C. Viscoelastic flow by the presence of radiation. *Zeitschriftfür Angewandte Mathematik und Mechanik (ZAMM)* **78**, 27–79, (1998).
- [34] Seddeek,M.A. Effects of radiation and variable viscosity on a MHD free convection flow past a semi-infinite flat plate with an aligned magnetic field in the case of unsteady flow. *Int. J. Heat Mass Transfer* **5**, 45–931, (2002).

- [35] Mabood,F., Imtiaz,M., Alsaedi,A.& Hayat,T. Unsteady convective boundary layer flow of Maxwell fluid with nonlinear thermal radiation: A Numerical study. *Int. J. Nonlinear Sci. Num. Simul* **9**, 17–221, (2016).
- [36] Hayat,T., Muhammad,T., Alsaedi,A.& Alhuthali,M.S. Magneto hydrodynamic three dimensional flow of viscoelastic nanofluid in the presence of nonlinear thermal radiation. *J. Magn. Magn. Mater* **9**, 222–385, (2015).
- [37] Farooq,M., Khan,M.I., Waqas,M., Hayat,T., A. Alsaedi& M.I. Khan MHD stagnation point flow of viscoelastic nanofluid with non-linear radiation effects. *J. Mol. Liq.* **103**, 221–1097, (2016).
- [38] Shehzad,S.A., Abdullah,Z., Alsaedi,A., Abbasi,F.M.& Hayat,T. Thermally radiative three-dimensional flow of Jeffrey nanofluid with internal heat generation and magnetic field. *J. Magn. Magn. Mater* **14**, 108–397, (2016).
- [39] Sheikholesmi,M.& Bhatti,M.M. Free convection of nanofluid in the presence of constant magnetic field considering shape effects of nanoparticles. *International Journal of Heat and Mass Transfer* **111**, 1039–1049, (2017).
- [40] UlHaq,R., Nadeem,S., Khan,Z.H.& Noor,N.F.M. Convective heat transfer in MHD slip flow over a stretching surface in the presence of carbon nanotubes. *Physica B* **457**, 40–47, (2015).
- [41] Talley,L.D., Pickard,G.L., Emery,W.J.& Swift,J.H. Descriptive Physical Oceanography, Physical Properties of Sea Water. *sixth ed., Elsevier Ltd* , 29–65, (2011).
- [42] Pastoriza-Gallego,M., Lugo,L., Legido,J.& Piñeiro,M. Thermal conductivity and viscosity measurements of ethylene glycol-based Al 2O3 nanofluids. *Nanoscale Res Lett.* **6**, 1–11, ().
- [43] Aberoumand,S.& Jafarimoghaddam,A. Experimental study on synthesis, stability, thermal conductivity and viscosity of Cu–engine oil nanofluid. *Journal of the Taiwan Institute of Chemical Engineers* **71**, 315–322, (2017).
- [44] Han,H., Jin,J.& Wu,X. A Finite-Difference Method for the One-Dimensional Time-Dependent Schrodinger Equation on Unbounded Domain. *Computers and Mathematics with Applications* **50**, 1345–1362, (2005).
- [45] Carnahan,B., Luther,H.A.& Wilkes,J.O. Applied numerical methods. *New York: John Wiley & Sons* , (1969).
- [46] Sobamowo,M.G. Finite element analysis of transient thermal performance of a convective-radiative cooling fin: effects of fin tip conditions and magnetic field. *Res. Eng. Struct. Mat.* **5**, 43–74, (2019).
- [47] Hering,R.G. Laminar free convection from a nonisothermal cone at low Prandtl numbers. *Int J Heat Mass Tran.* **8**, 1333–1337, (1965).
- [48] Thandapani,E., Ragavanand,A.R.& Palani,G. Finite difference solution of unsteady natural convection flow past a non-isothermal vertical cone under the influence of magnetic field and thermal radiation. *J ApplMech Tech Phy* **53**, 408–421, (2012).
- [49] Balla,C.S.& Naikoti,K. Finite element analysis of magnetohydrodynamic transient free convection flow of nanofluid over a vertical cone with thermal radiation. Proceedings of the Institution of Mechanical Engineers, Part N. *Journal of Nanoengineering and Nanosystems* **IMEchE** 1–13, (2014).